Size Distribution and Frustrated Antiferromagnetic Coupling Effects on the Magnetic Behavior of Ultrafine Akaganéite (β-FeOOH) Nanoparticles

*Carlos Luna,[*a] Maxim Ilyn,[b] Víctor Vega,[c] Víctor M. Prida,[c] Julián González[d] and Raquel Mendoza-Reséndez[e]*

[a] Centro de Investigación en Ciencias Físico Matemáticas (CICFiM) / Facultad de Ciencias Físico Matemáticas (FCFM), Universidad Autónoma de Nuevo León (UANL), Avda. Universidad S/N, San Nicolás de los Garza, Nuevo León, 66450, Mexico.

[b] Centro de Física de Materiales (CFM-CSIC), Pº Manuel de Lardizábal 5, 20018 San Sebastián, Spain.

[c] Depto. de Física, Facultad de Ciencias, Universidad de Oviedo, Calvo Sotelo S/N, 33007-Oviedo, Spain.

[d] Dpto. Física de Materiales, Fac. Quimicas, Universidad del Pais Vasco (UPV/EHU), Paseo Manuel de Lardizabal 3, 20018 San Sebastián, Spain.

[e] Facultad de Ingeniería Mecánica y Eléctrica (FIME), Universidad Autónoma de Nuevo León (UANL), Avda. Universidad S/N, San Nicolás de los Garza, Nuevo León, 66450, Mexico.

Corresponding Author: carlos.lunacd@uanl.edu.mx (C. Luna)

ABSTRACT

The magnetic properties of low dimensional materials of several iron oxyhydroxyde phases, such as akaganéite (β-FeOOH) or lepidocrocite (γ-FeO(OH)), remain poorly explored; probably due to their specific preparation as single crystalline phase requires special conditions owing to their structural instability. In the present work, ultra-fine akaganéite nanoparticles were prepared by the hydrolysis of $FeCl_3$ solutions at room temperature induced by the presence of NaOH. The resulting product was characterized by several analytical techniques. Structural investigations using X-ray diffraction (XRD), high-resolution transmission electron microscopy (HRTEM) and selected area electron diffraction (SAED) revealed that the sample was mainly constituted by rather-equiaxial akaganéite nanocrystals with mean diameter of 3.3 ± 0.5 nm. In addition, a small amount of rod-like akaganéite particles with 23 ± 5 nm in length and 5 ± 1 nm in width was also detected. The study of the respective dependences of the dc magnetization and the ac susceptibility on temperature and exciting magnetic field revealed complex magnetic relaxation processes, high coercivity values at low temperature and exchange bias effect. These results have been tentatively explained considering size distribution effects and the presence of superparamagnetic and spin glass-like contributions arising from the frustration of the antiferromagnetic order owing to surface effects and an insufficient filling of the akaganéite channels with Cl^- anions.

1. INTRODUCTION

The materials that constitute the iron oxide family (which, according to the tradition, includes iron hydroxides and iron oxyhydroxides[1]) are of key importance due to their extensive presence in nature and their functional properties.[1] Particularly, the wide variety of their magnetic responses, including ferrimagnetic, antiferromagnetic, weak ferromagnetic, superparamagnetic or speromagnetic behaviours,[1] which are closely correlated with the size, morphology and crystallo-chemical features of these materials, has attracted enormous attention for several decades. Moreover, some of the iron oxides exhibit interesting first-order magnetic phase transitions, such as the Morin transition found in hematite[2,3] and the Verwey transition discovered in magnetite.[4-6] However, it is remarkable that the research in iron oxides still remains subject of intense study and controversy, and the interpretation of some experimental results demand better refinements. In fact, the crystallographic properties and magnetic behaviors of some iron oxyhydroxides are subject of debate. One clear example of this is represented by the structural and magnetic properties of akaganéite (β-FeOOH), which is an iron oxide phase found in chloride rich environments. This iron oxyhydroxide displays a hollandite-like structure with edge- and corner-shared Fe(O,OH)$_6$ octahedra forming one-dimensional square hollows or channels that provide it interesting electrochemical and catalytic properties for a variety of practical applications.[7-9] Materials with this tunnel crystalline structure have been described with tetragonal or monoclinic unit cells (a schematic representation of akaganéite structure is showed in the inset of Figure 1). In pioneer studies of the β-FeOOH structure using X-ray diffraction and infrared spectroscopy, the tetragonal I4/m symmetry (a=10.48 Å, c= 3.023 Å) was assumed to describe the akaganéite crystallographic properties.[10-12] However, further

analysis with the Rietveld method of powder X-ray diffraction measurements, showed that the monoclinic I2/m symmetry describes better the akaganétite crystalline structure (a = 10.600(2) Å, b = 3.0339(5) Å, c = 10.513(2) Å, β = 90.24(2)°).[13] These results were subsequently corroborated by synchrotron X-ray measurements[14] and neutron diffraction experiments.[15]

Other open questions about the akaganéite structure are related to the role that plays the presence of chloride anions into the akaganéite crystalline lattice and its magnetic behavior. Results from several works have indicated that the occupancy of these ions into the channels is crucial for the formation of akaganéite.[10-15] However, there is not yet a well-established consensus about how is the occupancy distribution of these ions into the channel sites, which is crucial to the charge balancing of the structure. Several works have suggested that the Cl⁻ ions are periodically located with a sequence of two consecutive channels filled and a third site vacant, being the reported X-ray diffraction, Mössbauer and synchrotron data in agreement with 2/3 Cl populated sites.[13,14,16] Note that assuming that Cl ions are placed in (0,0,0), the Cl-Cl distance should be equal to the b lattice parameter (around 3 Å), which is shorter than the Cl ionic radius (3.6 Å).[14] However, some studies have pointed out that a more realistic description should consider shifts in the y-coordinate of the Cl sites and few additional vacancies randomly distributed.[14] These differences in the description of the crystallo-chemical properties of akaganéite have provoked controversy in the interpretation of the Mösbauer spectra (summarized in the introduction of ref. 16), because some of them considered the tetragonal unit cell in their interpretations[12,17] while others the monoclinic cell.[14,16] In addition, different locations of the chloride ions have been considered.

Generally, it has been assumed that bulk akaganéite behaves like an antiferromagnet,[1] where two spin sublattices are antiferromagnetically coupled parallel to the one-dimensional channels (along the b direction of the monoclinic I2/m representation). However, akaganéite exhibits some features that would become it an unconventional antiferromagnet. For instance, in the thermal dependence of the akaganéite susceptibility it was not observed the typical well-defined maximum near the Néel temperature, T_N.[18,19] Moreover, it has been found that the determination of this temperature strongly depends on the used methodology and the characteristics of the analyzed specimens. For example, based on the observation of an doublet or a sextet in the Mössbauer spectra, several works have determined that T_N of the bulk akaganéite is around 295 K,[12,20] while other works reported lower values based on magnetic susceptibility measurements[19] (for example, $T_N \sim 260$ K), in which the determination of T_N is based on the occurrence of a weak peak[18] or deviations from the Curie-Weiss law[19] in the thermal dependence of the magnetic susceptibility. Notice that in these experimental methodologies used to determine the Néel temperature, the magnetic disorder-order transition could be partially concealed by weak ferromagnetic-like contributions and/or confused with magnetic blocking or spin glass freezing processes. Therefore, the experimental observations could suggest that bulk akaganéite does not exhibit a pure antiferromagnetic behavior. In this matter, the occurrence of several magnetic contributions has been proposed in the explanation of akaganéite Mössbauer spectra invoking four un-equivalent iron sites into the akaganéite crystal lattice: the monoclinic structure involves two un-equivalent iron sites, which lead to four un-equivalent Fe locations if it is considered the occupancy (or vacancy) of chloride ions close to these sites, where the octahedra closest to chlorine ions are more distorted.[16] Consequently, the Cl^- occupancy should display an important influence on the exchange coupling between the spin sublattices and the

resulting magnetic behavior,[16,21] however it is not well-established what is the role of the chlorine ions. In this respect, Chambere and Grave found that the Néel temperature decreases as the increment of the crystal water content increases,[22] which implies a reduction of Cl^- content,[21] and Millan et al.[21] proposed that a faulty of Cl^- site occupancy yield to alterations in the antiferromagnetically spin alignment resulting a small net magnetic moment. Therefore, a Cl^- ion vacant distribution should introduce spin disorder and variations from site to site of the easy magnetization direction. In agreement with this hypothesis, Coey[23] proposed a speromagnetic model in all iron oxyhydroxydes instead antiferromagnetism, and more recently, Barrero et al.[16] have suggested that the akaganéite magnetic structure consists of two asperimagnetic-like structures antiferromagnetically coupled.

It is noticeable that the chloride content and other microstructural features of akaganéite samples could be strongly dependent on the route in which they were obtained and purified, and their size and shape if they are constituted by small particles. In this regard, it is important to emphasize that the specimens used in the reported micro-structural and magnetic studies of akaganéite, have been obtained by very different methods. In this way, in some of these contributions, the investigated samples were extracted from meteorites,[11,13] whereas other works used samples biosynthesized by bacteria[24] or prepared by thermal hydrolysis of $FeCl_3$ solutions aged at temperatures between 70 and 100°C during several hours.[1,8-10,12,16,21] In the two later cases, the samples usually are formed by nanosized particles with a flattened rod-like shape. Therefore, the effects of the lattice symmetry breaking and broken bonds at the crystal surface, which represent another source of disorder and frustration of antiferromagnetic interactions,[21,24,25] could be not negligible due to the high surface/volume ratio of nanoparticles.

To the best of our knowledge, there are few reports in the literature focused on the study of surface and finite-size effects on the magnetic properties of nanosized akaganéite particles [for example, references 19, 21]. In the present contribution, we report on the magnetic properties of ultrafine akaganéite nanoparticles prepared by hydrolysis of Fe (III) solutions at room temperature. Most of the particles obtained through this synthesis method were nearly spherical in shape, which is a morphology rarely observed in nanoscale akaganéite. In the interpretation of the results, the possible contribution of particle size distribution, interparticle interactions, magnetization quantum tunneling and frustration of spin interactions were evaluated.

2. EXPERIMENTAL SECTION

i) Chemicals

Anhydrous iron (III) chloride ($FeCl_3$, 97 %, Sigma-Aldrich), sodium hydroxide (NaOH, 98%, J. T. Baker) and absolute ethanol (Sigma-Aldrich) were used with the as received purity. The water added in all experiments was doubly distilled.

ii) Preparation of akaganéite nanoparticles

Nanosized akaganéite particles were prepared by the hydrolysis of aqueous iron (III) chloride solution at room temperature. This one-step preparation of an akaganéite colloid consisted in the simple following procedure based on the results of previous works.[26] Briefly, 25 ml of 2 M aqueous solution of $FeCl_3$ were rapidly added to 30 ml of 5 M aqueous sodium hydroxide solution under vigorous and continuous stirring using a stirring plate at room temperature.

Immediately, the solution changed its color and it acquired a yellowish brown, suggesting the formation of an iron oxyhydroxide colloidal suspension. After ten minutes, the resulting suspension was diluted with absolute ethanol and centrifuged. The supernatant solution was removed and the precipitated powder was washed several times with doubly distilled water, absolute ethanol and centrifugation. Finally, the so-prepared powders were dried at 50°C during 5 hours. The obtained particles were not subjected to posterior aging process at temperatures close to 100ºC as in previous works.[26]

iii) Characterization Techniques

The crystalline phase of the sample was identified by powder X-ray diffraction (XRD), using a Panalytical Empyrean diffractometer. This difractometer is equipped with a graphite monochromator on the diffraction bean and a X´Celerator linear detector. The difractometer was calibrated with a silicon standard sample. Cu Kα_1 X-ray radiation (λ =1.5405980 Å) was generated from a Cu anode and was set up on 45 kV and 40 mA. Data were collected at room temperature in the 2θ range between 19.996 and 90.000°, with a scan step size of 0.017°. The mean coherence lengths (MCL) perpendicular to some crystallographic planes of the sample were calculated from the full width at half maximum of the corresponding XRD peak using the Scherrer equation:[27]

$$MCL = \frac{0.9\,\lambda}{\beta\,Cos\,\theta_B} \tag{1}$$

where λ is the X-ray wavelength, β is the broadening of the diffraction peak (after subtracting the instrumental broadening) and θ_B is the diffraction angle associated to each peak.

The particle size and morphology of the sample were examined by Transmission Electron Microscopy (TEM) using a FEI-TITAN 80-300 kV microscope operated at 300 kV. The average size and size distribution of the particles were determined by statistical analysis of the dimensions observed in the TEM micrographs of more than 100 particles. In addition, High Resolution Transmission Electron Microscopy (HRTEM) and Selected Area Electron Diffraction (SAED) studies were carried out in order to gain further information about the nanoparticle microstructure. HRTEM images were analyzed by fast Fourier transform (FFT). For the TEM analysis, the synthesized powder was dispersed in ethanol by ultrasonification and a drop of the resulting suspension was deposited onto a lacey carbon TEM grid of copper.

A commercial vibrating sample magnetometer (Quantum Design) was used to investigate the magnetic behavior of the samples by applying dc magnetic fields (with a maximum applied field of 70 kOe). The thermal dependencies of the zero-field cooled (ZFC) and field-cooled (FC) magnetizations were measured in the range of 1.8-300 K under variable external magnetic fields (from 100 Oe up to 70 kOe). These measurements were performed according to the following procedure. Firstly, the sample was cooled from room temperature (RT) down to 1.8 K in zero applied field. Then, in order to obtain the ZFC curve, an external field was applied and the variation of the magnetization was recorded with temperature increasing from 1.8 K up to RT. Afterwards, to obtain the FC curve, the magnetization was reordered as a function of temperature by cooling the sample down to 1.8 K keeping the same applied field. The cusp temperatures of the ZFC curves obtained with different applied field were determined by using the first derivative test (dM/dT vs T). The thermoremanent (TRM) curve was measured as follows. Firstly, the sample was cooled from RT down to 1.8 K in a field of 100 Oe. At the lowest

temperature value the field was removed and then, the remnant magnetization was measured as a function of temperature for increasing temperatures in zero field. The isothermal magnetization versus magnetic field curves where measured at different temperatures in the range of 1.8-300 K by sweeping the applied field from 70 to -70 kOe and back to 70 kOe. In these measurements, the sample was cooled from 300 K down to the measurement temperature in absence of magnetic fields (ZFC condition), or in presence of 70 kOe (FC condition). In the case of the ZFC hysteresis loop obtained at 1.8 K, the first magnetization curve was also recorded.

The coercive field, H_C, and the exchange bias field, H_{EB}, were estimated from hysteresis loops using the following expressions:

$$H_C = \frac{H_C^+ - H_C^-}{2} \quad , \quad H_{EB} = \frac{-\left(H_C^+ + H_C^-\right)}{2} \tag{2}$$

where H_C^- and H_C^+ represent the fields at which the magnetization becomes zero in the loop´s branches ascribed to the negative and positive field sweeping, respectively. To determine the magnetic viscosity, S, the sample was previously saturated by applying a positive field (2T). Then, the magnetic field was abruptly removed and the magnetization was measured as a function of the time. This measurement was repeated at different temperatures (from 3 to 15 K) and the S values were obtained by fitting the experimental M vs time curves to the following equation:

$$M(t) = M(0) - S \ln(t) \tag{3}$$

The in phase component (i.e. the real part, χ') and the out of phase component (i.e. the imaginary part, χ'') of the ac susceptibility were both simultaneously measured at 21 different frequencies, ν, in the range of 100-10,000 Hz and at the temperature range of 5-100 K in absence of dc fields using a PPMS (Physical Property Measurement System), model 6000 (Quantum Design). The data were recorded following the next procedure. Firstly, the sample was cooled from room temperature to 5 K in the absence of exciting magnetic fields. Then a probing ac magnetic field of amplitude 2 Oe was applied with frequencies varied from 10 up to 10,000 Hz. Afterwards, the same measurements were carried out at higher temperatures up to 101 K in steps of 2K. The cusp temperatures of the χ' vs T and χ'' vs T curves were accurately determined as the temperature at which the corresponding first derivative curve changes of sign.

3. RESULTS AND DISCUSSIONS

i) Microstructural and morphological studies

Figure 1 shows the X-ray diffraction (XRD) pattern of the sample. It consists on rather broad peaks that can be resolved and ascribed to a pure akaganéite phase (JCPDS card No. 42-1315). The peak broadness evidences the ultra-fine crystal size of the sample, and the peak positions indicate that the sample exhibits lattice parameters close to the bulk ones: a = 10.492(9) Å and c = 3.066(6) Å, for the tetragonal cell description, and a =10.60(4) Å, b = 3.04(1) Å, c = 10.47(4) Å and β = 89.4(6)°, for the monoclinic unit cell description. The crystallite size determined from the MCL of the diffraction peak more intense was 3.0(2) nm. It is remarkable, that the relative diffraction peak intensities in the XRD pattern of the sample are not the same than those of the

reference pattern, probably due to the atypical equiaxial morphology of the ultrafine particles studied herein. Also, the akaganéite structure was confirmed by SAED analysis. Inset of Fig. 2a shows a typical pattern of several nanoparticles that are constituted by slightly diffused diffraction rings consistent with the akaganéite structure and the extremely reduced crystal size of the sample.

TEM studies revealed that the sample is constituted by nanoparticles nearly spherical in shape with an average diameter of 3.3 ± 0.5 nm, whose difference with the estimated average crystal size is within experimental error. In addition, a minor presence of very small rod-like particles with 23.4 ± 5.1 nm in length and 4.9 ± 1.4 nm in width was clearly detected (see Fig. 2a). Fig. 2b depicts a typical HRTEM micrograph, where lattice fringes ascribed to the monoclinic akaganéite structure are observed (see the insets of the Fig. 2b), whereas lattice fringes of additional phases were not found confirming that the akaganéite phase is the only single crystalline phase present in the sample.

Figures 2c and d show the histograms of the effective particle diameter of both particle families. In the case of the second family, the effective diameter of each studied nanorod was determined with the half sum of its length and width. It is well known that the akaganéite nanoparticles tend to exhibit somatoidal, rod-like or even tubular morphologies,[1,16,19,21,24] whose formation mechanism could consist on the precipitation of primary equiaxial nanoparticles with sizes around 3–4 nm, followed by their rapid growth in the direction of c-axis, and a secondary nucleation occurring at sites on the edges.[26] Therefore the particles studied herein (that were not subjected to aging effects at temperatures close to the boiling point of water) are in the first stage

of the growth of the elongated particles. An interesting point to note is that after storing the sample in powder form at room temperature during one year, the specimen was not experienced significant changes in the particle morphology and/or its crystallinity (Fig.1 shows the DRX pattern of the aged sample in comparison with the fresh sample one).

ii) Magnetic studies

The thermal dependence of the inverse of the dc magnetic susceptibility, $1/\chi$, measured in a constant magnetic field of 100 Oe is showed in Fig. 3. The complex behavior of this curve suggests that the sample experiences changes in their magnetic behavior with the variation of the temperature. In fact, three different regimes, associated to the temperature intervals: a) 1.8-40 K, b) 40-260 K and c) 260-320 K, can be distinguished.

At temperatures above the Néel temperature, the magnetic susceptibility of a bulk antiferromagnetic material should follow the Curie-Weiss law[28]

$$\chi^{-1} = \frac{T - \theta}{C} \tag{4}$$

where T is the temperature and θ and C are the Weiss and Curie constants, respectively. In the case of the nanosized akaganéite studied herein, we observe that the best fit curve of the experimental data to equation (4) in the temperature range from the maximum reported Néel temperature for bulk akaganéite (295 K) up to 320 K, deviates from the experimental values at temperatures below 260 K (Fig. 3). It suggests that the average Néel temperature ascribed to the particles is around 260 K, which is the same value reported by Urtizberea et al. for bulk akaganéite and very fine akaganéite nanorods.[19]

Astonishingly, the best fit of the data to equation (4) in the temperature range of 295-320 K implies a positive Weiss constant (see Fig. 3), as it is expected for ferromagnetic materials and not for pure antiferromagnetic systems. It indicates that in the sample coexist several magnetic phases. In fact, the non-observance of a maximum near T_N in the thermal dependence of the susceptibility in Fig. 3 suggests the occurrence of additional weak ferromagnetic-like or superparamagnetic contributions, which should arise from non-compensated spins, and which partially conceals the rapid change of the magnetization at temperatures close to T_N.

Two possible different sources of antiferromagnetic coupling frustration can be present in small akaganéite particles.[21] One of them would be related to the imperfect antiparallel alignment of spins given by a deficient occupancy of chloride ions into the akaganéite channels,[21] as above mentioned. The other one is ascribed to surface effects. In ultrafine particles, most of the atoms lie at particle surface, where the coordination number displays a distribution with values more reduced than in volume, and the antiferromagnetic alignment becomes geometrically frustrated. Both kinds of sources of uncompensated spins and magnetic disorder should yield to relaxation phenomena at low temperatures, whose contributions should be strongly dependent on the particle size and shape. The resulting disordered magnetic structure of each particle should originate multiple degrees of freedom leading to a configuration of several equivalent fundamental states, which give rise to spin glass-like behaviors. We assume that the effects of the phenomenon named *thermoinduced magnetic moment*, proposed by Mørup and Frandsen for antiferromagnetic materials[29] and very recently studied in akaganéite nanorods,[19] are negligible in our particle system due to its large fraction of uncompensated spins.

According to these considerations, in the temperature range from 260 K up to 320 K, the antiferromagnetic spins would exhibit a paramagnetic behavior, whereas the uncompensated spins would be in a superparamagnetic-like regime. At temperatures in the range 40-260 K, the values of $1/\chi$ monotonically decrease as temperature decreases with a lower ratio than that at higher temperatures. It suggests that in this low temperature range, the spins antiferromagnetically coupled experienced a paramagnetic-antiferromagnetic transition, whereas the uncompensated spins remain into a superparamagnetic regime. Finally, at temperatures between 1.8-40 K, $1/\chi$ exhibits a maximum at ~ 21 K (see the inset of Fig. 3), suggesting that the uncompensated spins experience a blocking (or a magnetic freezing) process when the temperature decreases.

The plots of M vs H/T (Fig. 4) at fixed temperatures confirmed the existence of several magnetic regimes: at temperatures above 100 K, these curves are roughly coincident in fair agreement with a paramagnetic (or superparamagnetic) behavior.[30] However, deviations from this coincidence were observed in the temperature range between 20 and 100 K, being more relevant as temperature decreases below 50 K, signaling the start of a magnetic blocking or freezing process, and/or an increase in the importance of interparticle interaction effects at low temperature that yields to deviations from a pure superparamagnetic behavior.[31] At temperatures below 20 K, the sample presented magnetic hysteresis indicating that a large fraction of the spins are blocked (or frozen).

The experimental M vs H curve measured at 300 K was fitted to the Langevin function, corresponding to the paramagnetic regime:

$$M(a) = M_S \left| Coth(a) - \frac{1}{a} \right| \qquad (5)$$

with a=μH/k_BT, where k_B is the Boltzmann constant, M_S the saturation magnetization in emu/g and μ is the net magnetic moment per particle. The best fitting parameters were M_S = 15.1 ± 0.1 emu/g and μ = 143 ± 2 μ_B. Since each Fe^{3+} ion has a magnetic moment of 5 μ_B,[32] we can expect an average uncompensated spin number per particle n_{unc} ≈ 29. The number of uncompensated spins distributed on the particle surface can be estimated from the total number of spins per particle (n), $n_{unc,surface}$ ≈ $n^{1/3}$.[19] For akaganéite, there are 2.5 x 10^{22} Fe^{3+} ions per cm^3 therefore, for a spherical particle with a diameter of 3.3 nm, n ≈ 3,763 and $n_{unc,surface}$ ≈ 16, which is around the half value of n_{unc}. The difference between the estimated values of n_{unc} and $n_{unc,surface}$ is in agreement with the occurrence of uncompensated spins in the particle volume, however it is important to remark that in these simple estimations we have not considered crucial factors such as size distributions and deviations from the spherical morphology.

Figure 5 shows the zero-field-cooling (ZFC) and field-cooling (FC) magnetization curves for different applied magnetic fields. These curves present several typical features associated to small single-domain nanostructures[33,34] and very small antiferromagnetic nanoparticles.[35,36] Specifically, it is observed that the ZFC and FC curves measured at high values of the applied magnetic fields (H ≥ 30 kOe) are roughly coincident in the entire studied temperature range (1.8-300 K). However, these curves split below certain temperature for H < 30 kOe, called irreversibility temperature (T_{irr}); whereas the FC magnetization increases as temperature decreases, the ZFC magnetization decreases reaching a peak at a temperature T_p (see Fig. 5). These behaviors indicate that a magnetic blocking[30,34] (or a magnetic freezing[33,35,36]) process

occurs in the system when the temperature decreases from RT down to low temperatures, which is associated to the uncompensated spins arisen from the frustration of the antiferromagnetic coupling. According with these considerations, the peak temperature (T_p) at which the maximum of the ZFC curve occurs for a low value of the applied magnetic field, T_p(H=100 Oe) = 34.5 ± 0.1 K, could be related with the average blocking temperature, T_b (or spin-glass freezing temperature, T_f) of the uncompensated spins. On the other hand, the T_{irr} could be ascribed to the blocking temperature (or spin-glass freezing temperature) of spins with highest energy barrier.[33]

The field dependences of T_p and T_{irr} are reported in Figure 6. For uniaxial single-domain nanoparticles, the blocking temperature is[30]

$$T_b = U / [k_B \ln(t_m/\tau_0)] \tag{6}$$

where U is the anisotropy energy, k_B is the Boltzman constant, t_m is the measuring time of the employed characterization technique and τ_0 is the attempt time. On the other hand, the energy barrier U can be modified by the applied magnetic field, H, as follows:

$$U = K_A V(1-H/H_K)^2 \tag{7}$$

where K_A is the anisotropy constant, V the particle volume and $H_K = 2K_A/M_S$ is the anisotropy field (M_S is the saturation magnetization). Therefore, T_b should decrease monotonously as H increases.[37] Interestingly, the curve T_p vs H in Fig. 6a does not follow a $(1-H/H_K)^2$ law, and the change rate is considerably lower at magnetic fields H < 1 kOe than that at higher fields.

Moreover, the T_p vs H curve only follows the so-called Almeida-Thouless (A-T) line for fields H > 5 kOe (Fig. 6a). The A-T line is usually observed for spin glasses and nanoparticles with spin-glass-like behaviors,[38-40] and is given by:

$$H \propto (1-T_p/ T_g)^{3/2} \qquad (8)$$

where T_g is the spin glass transition temperature. On the other hand, T_{irr} values present a non-monotonic dependence showing a maximum at H = 0.50 kOe.

In some nanoscale magnetic materials, it has been found that T_P (and/or T_{irr}) firstly increases with increasing field until it reaches a maximum, and then it decreases.[41,42] Usually, this behavior has been related to the resonant magnetization tunneling effect.[41,42] However, computational simulation results have showed that the T_P vs H curve of uniaxial magnetic nanoparticle assemblies could adopt a bell-like shape when their energy barriers are log-normal distributed[37,43] due to log-normal distributions of the particle size[43] and/or the existence of weak interparticle magnetostatic interactions.[33,44] Under these circumstances, the average blocking (or freezing) temperature could be rather different than the maximum observed in the ZFC curve obtained in presence of lower magnetic fields.[43] In agreement with this, we observe that T_p(H=100 Oe) $\approx$ 34.5 K is considerably larger than the minimum temperature (~20 K) above which no magnetic hysteresis was found. Therefore, both dependences of T_p and T_{irr} could be explained assuming that the blocking (freezing) temperature distribution displays several contributions with different field-dependencies that yield to a distribution of energy barriers with a field-dependent width. In our nanoparticles, the blocking (or freezing) temperatures should

display a wide distribution owing to the presence of two particle populations with different shapes (a predominant population of rather-spherical nanocrystals together a minority quantity of nanorods), in which several relaxation mechanisms ascribed to two different sources of antiferromagnetic exchange coupling frustration (one ascribed to surface effects and other one associated to the Cl^- ion vacancy effects) take place.

In order to check this conjecture, the thermoremanent magnetization (TRM) was measured with a magnetic field of 100 Oe as a function of temperature (see the inset of Fig. 7a). The corresponding derivative vs temperature has been associated to the energy barrier distribution for non-interacting[45] and interacting magnetic nanoparticles[33], and also for antiferromagnetic small particles.[46] This curve for ultrafine akaganéite nanoparticles (Fig.7a) confirms the coexistence of several energy barrier contributions with the presence of a shoulder before reaching its maximum value, and it was satisfactorily described (R^2 = 0.9989) as the sum of two log-normal distributions with central values 8.1(4) and 14.37(9) K and standard deviations of 0.73(2) and 0.37(1), respectively. Note that, the height of this curve decreases down to the 34% of the maximum height at around 20 K (i.e. the maximum temperature at which the sample present magnetic hysteresis).

On the other hand, the thermal dependence of the derivative of the difference between FC and ZFC magnetization with respect to temperature, $- d(M_{FC} - MZ_{FC}) / dT$, also represents the anisotropy energy barrier distribution of the system,[33,40] offering the possibility to study its dependence on the magnetic field. Fig. 7b-f depict these curves obtained at different applied magnetic fields, and are compared with the derivative of the TRM curve vs temperature. The

former curve is very similar to the $- d(M_{FC} - MZ_{FC}) / dT$ vs T one obtained at H = 100 Oe, confirming the direct relation between both curves. The $- d(M_{FC} - M_{ZFC}) / dT$ vs T curves were also fitted to the sum of two log-normal distributions (named 1 and 2 in Fig. 7b-f) whose fit parameters are represented as a function of H in Fig. 8a-c. The temperatures at which the maxima occur for both distributions (T_{C1} and T_{C2}, respectively) tend to decrease when H increases (Fig. 8a). The distribution 1 tends to vanish at H > 5 kOe, suggesting that the average anisotropy field associated to this energy barrier distribution is around 5 kOe. At H > 5 kOe, the total energy barrier distribution becomes considerably narrower and a small increase of the ZFC magnetization is observed as temperature decreases in the lowest temperature range (see Fig. 5). On the other hand, the ZFC-FC curves are roughly coincident at H = 30 kOe, indicating that the average anisotropy field associated to the distribution 2 is close to 30 kOe (approximately twice the value for bulk β-FeOOH recently estimated by Urtizberea et al.[19]). Noteworthy, the standard deviations (σ_1 and σ_2, Fig. 8b) and the amplitude (A_1 and A_2, Fig. 8c) of both log-normal distributions are field-dependent.

In order to estimate the importance of the magnetostatic interparticle interactions on the magnetic behavior of the system, the mean dipole-dipole interaction energy between two neighboring spherical particles was roughly estimated using the following equation:[39,47]

$$E_{d-d} = \frac{\mu_0}{24} M_S^2 d_m^3 \varepsilon \qquad (9)$$

where M_S is the saturation magnetization of the particles, d_m is the median particle diameter and ε is the particle concentration by volume. Assuming M_S = 50 kA/m, d_m = 3.3 nm (the mean size

of the equiaxial nanoparticles) and $\varepsilon = 63.4$ % (the maximum density for a random packing), we obtain $E_{d-d} / k_B \approx 0.24$ K, (i.e., around two order of magnitude lower than T_P at H=0.1 kOe). The size of nanorods is considerably larger than 3.3 nm, however their concentration by volume is substantially lower than the equiaxial particles. In this manner, estimations using equation (9), and assuming $d_m \approx 16$ nm and $\varepsilon < 20$ % gives E_{d-d} / k_B values largely lower than T_P at H = 0.1 kOe. Hence, this crude approximation indicates that the interparticle interaction effects have not an important contribution on the blocking/freezing processes.

For nanoparticles of antiferromagnetic materials it has been observed that the temperature of the peak in ZFC magnetization measurements decreases with increasing the particle size,[35,48] which is the contrary tendency observed in nanoparticles of ferromagnetic (or ferrimagnetic) materials.[33] Hence, assuming that interparticle intaractions have not a relevant contribution, we attributed the log-normal distribution 1 to the barrier energy distribution of the akaganéite nanorods and the distribution 2 to the barrier energy distribution of equiaxial ultrafine particles.

In order to analyze the possible contribution of the quantum tunneling of magnetization to the magnetic relaxation of the sample, additional studies were carried out. In this respect, it is important to have in mind that antiferromagnetic nanosized systems with a small magnetic moment originated by the non-compensation of collinear spin sublattices are considered as more suitable experimental models than ferromagnetic nanoparticles to study this quantum phenomenon.[42] The temperature of the crossover from thermal to quantum regime can be estimated through the following expression:[42]

$$T_{Cr} = \frac{gk_B\sqrt{2H_AH_E}}{2\pi k_B} \quad (10)$$

where g is the landé factor, μ_B is the Bohr magneton, k_B the Boltzmann constant and H_A and H_E are the anisotropy and exchange fields, respectively. Assuming the values of H_A and H_E of bulk akaganéite recently reported by Urtizberea et al.,[19] the estimated value is $T_{Cr}\sim$ 5K, which is of the same order (or even larger) than the T_C value obtained for ferritin.

Figure 9 shows the thermal dependency of the magnetic viscosity. In this curve, the S values increase as temperature decreases in the whole explored temperature range. Therefore, the temperatures at which the viscosity is not temperature-dependent due to the occurrence of quantum relaxation phenomena[49] is significantly lower than the temperatures at which measurements were carried out. Consequently, the experimental value of T_{Cr} is significantly lower than the estimated value, probably due to the wide distributions of H_A and H_E of our akaganéite nanoparticles, being the mean value of H_E drastically smaller than that of the corresponding one for the bulk β-FeOOH owing to their ultrafine size and surface effects.

Figures 10a and b show the temperature dependence of in-phase, χ', and out-of-phase, χ'', ac susceptibility components measured at selected frequencies. In all these curves, a well-defined frequency-dependent peak is clearly observed confirming the occurrence of a magnetic blocking or freezing process. Interestingly, the frequency dependence on the temperature of the peak is rather different than the usually found in non-interacting superparamagnetic particles,[39] spin glasses,[50] surface spin glasses[35] and super spin glasses,[39,47] where the temperature of the peak increases as the frequency is increased. In fact, the both cusp temperatures of χ' and χ'' of the analyzed akaganéite nanoparticles, which were named as T_{max1} and T_{max2} respectively, present a

non-monotonous dependence with the ac field frequency (see Fig. 11a-b). This behavior is in agreement with the occurrence of several magnetic relaxation mechanisms with different thermal dependences (see the discussion above about T_p and T_{irr}). Figures 12a and b presents the Cole-Cole plot of χ'' vs χ' at different temperatures. The asymmetric shape of these curves corroborates the coexistence of several relaxation time distributions.

Figures 13a and b show the dependence of the isothermal magnetization on the magnetic field measured at different temperatures. All these curves display a linear behavior at high values of the applied field, ascribed to the presence of spins with antiferromagnetic ordering and paramagnetic-like contributions. The magnetization values found at high magnetic fields were considerably larger than those reported in the literature for akaganéite nanoparticles and bulk akaganéite,[19, 21] indicating an unusual enhanced fraction of uncompensated spins in agreement with the extremely reduced dimensions of our nanoparticles. At temperatures above 20 K no magnetic hysteresis was found. However, hysteresis loops with rapidly increasing coercive fields as temperature decreases were observed at temperatures below 20 K. The found thermal dependence of the coercive field at low temperatures was not satisfactorily described by models taking into account non-interacting identical single domain particles with uniaxial anisotropy (see Fig 14), where it is expected the following relation:

$$H_C(T) = H_C(0)\left[1 - \left(\frac{T}{T_B}\right)^{\kappa}\right] \tag{11}$$

being H_C (0) the coercive field at T= 0 K, T_B the blocking temperature of the system, and k is 0.5 when the magnetic anisotropy axes of the particles are aligned or 0.77 when the particles are randomly oriented.[51] The parameters of the best fit (R^2 = 0.99763) of the experimental data to equation (11) with k as a free fit parameter, were H_C (0) = 7.5(2) kOe, T_B = 13.9(5) K and k =

0.181(6). On the other hand, the hysteresis loops presented typical characteristics observed in the hysteresis loops of very small antiferromagnetic nanoparticles: they are not fully saturated and display large coercivity and irreversibility at high fields (around 20 kOe).[35,36,46] Additionally, these hysteresis loops appear shifted along the magnetic field axis when they are measured after field cooling, suggesting the exchange coupling between the uncompensated spins together with the compensated ones.[36,46] However, the found values of the exchange bias field (for example, $H_{EB} \approx 354$ Oe measured at 1.8 K after cooling the sample under a magnetic field of 7 T) are quite low in comparison with the reported ones for several antiferromagnetic nanoparticle systems, which are typically of the order of few or even tens of kOe.[36,46] On the other hand, the coercive fields of the FC hysteresis loops were roughly the same as those obtained in ZFC hysteresis loops, therefore, the other typical manifestation of the exchange anisotropy consisting on the broadening of the magnetic hysteresis loops measured under FC conditions[52] was very modest. This moderate character of the exchange bias effect is consistent with a very limited presence of antiferromagnetically compensated spins in each particle owing to the ultrafine size of the nanoparticles studied herein.

Another interesting feature of the hysteresis loops of akaganéite nanoparticles was the occurrence of small "jumps" of the magnetization at low fields in both branches (see Fig. 13b and the sharp peak of the dM/dH vs H curve at H=0 in the inset of Fig. 13a). Similar noticeable magnetization jumps at low fields have been reported in several experimental studies of different nanoparticle systems, and they have been associated to different phenomena. For instance, Friedman et al.,[41] reported on magnetic hysteresis loops at low temperatures in ferritin exhibiting an anomalous "pinched" shape at near zero field. These authors attributed this effect to quantum

tunneling of magnetization that implies that the magnetic relaxation should be faster in zero field than at low applied field values.[41] Ong et al.[53] found noticeable magnetization jumps in both branches of the hysteresis loops in Fe/Fe_3O_4 core-shell and Fe_3O_4 hollow-shell nanoparticles, and these authors attributed them to a sudden switching of shell magnetic moments. Ammar et al.[54] observed similar jumps in the hysteresis loops of cobalt ferrite nanoparticles when they are not enough dispersed in a matrix, and these authors attributed such jumps as a consequence of the interparticle interactions, however the mechanism in which it should occurs was not explained. The same phenomenon was observed by Caldero-DdelC et al. in similar samples, and they suggested that magnetization jumps could occur due to rigid body rotation of the particles when the applied field direction is switched during measurement.[55] In the case of our akaganéite nanoparticles, the low field demagnetizations at 1.8 K normalized with respect to the magnetization measured at 70 kOe, $\Delta M/M_{7K}$, were 2.15 and 2.20 % for the branches ascribed to the negative and positive field sweep, respectively, measured in ZFC conditions. These jumps were less marked as the temperature was increased (for example, 1.67 and 1.56% at 5 K, and 1.11 and 1.11 % at 10 K) until becoming negligible. Interestingly, these demagnetization jumps were higher when the hysteresis loops were performed in FC conditions (for instance, 3.50 % at 1.8 K for both field sweep) and this effect was not observed in the first magnetization curves of the ZFC hysteresis loops. These discoveries suggest that a small population of uncompensated spins reverses before the whole. The demagnetization jumps are more marked in FC hysteresis loops probably due to the distribution of the spin tilting angle with respect to the direction of the exciting field should be narrower when the uncompensated spins are frozen in presence of a magnetic field. The existence of populations of spins with different switching fields is consistent with the wide distributions of the exchange and anisotropy fields (mentioned above) owing to the

particle size and shape distributions, and the distributions of the coordination number at the particle surface and of Cl^- occupancy in both particle populations (rather spherical ultrafine particles and nanorods). On the other hand, the occurrence of these jumps should be vanished for nanoparticle systems with strong magnetic interactions, confirming that there is not an important effect of interparticle interactions in our system. In this matter, simulations of fine magnetic particles have predicted jumps in the magnetization originated by the influence of the surface anisotropy, where each jump is related to a particular set of spins reversing, and their observation is strongly depend on the ratio of the intensity of the interparticle interaction and the strength of the surface anisotropy.[56]

CONCLUSSIONS

The hydrolysis of $FeCl_3$ solutions at room temperature induced by the presence of NaOH, and without further thermal treatments, yields to the formation of ultrafine akaganéite particles. Such nanoscale system is mainly constituted by rather-equiaxial β-FeOOH nanocrystals with diameters around 3.3 nm and by a small fraction of rod-like particles with 23 ± 5 nm in length and 5 ± 1 nm in width. These particles exhibit an interesting magnetic phenomenology that includes superparamagnetic-like behaviors, anomalous field dependences of T_p and T_{irr}, magnetic hysteresis at low temperatures with small "jumps" of the magnetization at low field values and exchange bias. This complex phenomenology has been explained considering the presence of two particle populations (rather equiaxial and rod-like particles) and the coexistence of antiferromagnetically coupled spins and uncompensated spins in a freezing magnetic state at low temperatures. The partial breakdown of the antiferromagnetic order is produced by two

sources of frustration of antiferromagnetic interactions and magnetic disorder: i) the geometrical frustration of the antiferromagnetic coupling produced by the reduced coordination number and structural disorder at the particle surface, where the breaking of the crystal lattice symmetry occurs, and ii) a deficient occupancy of chloride ions into the akaganéite structure channels that yields to an imperfect antiparallel alignment of spins (frustration by spin canting) resulting in a net magnetic moment. The effects of interparticle interactions and quantum relaxation phenomena apparently have not a notorious contribution in the observed magnetic behaviors.

ACKNOWLEDGMENTS

REFERENCES

[1] Cornell, R. M.; Schertmann, U. *The Iron Oxides*, 2nd Ed; Wiley-VCH: Weinheim 2003.

[2] Morin, F. J. Magnetic Susceptibility of α-Fe$_2$O$_3$ and α-Fe$_2$O$_3$ with Added Titanium *Phys. Rev.* **1950**, *78*, 819-820.

[3] Luna, C.; Vega, V.; Prida, V. M.; Mendoza-Resendez, R. Morin Transition in Hematite Nanocrystals Self-Assembled Into Three-Dimensional Structures. *J. Nanosci. Nanotechnol.* **2012**, *12*, 7571-7576.

[4] Verwey, E. J. W. Electronic Conduction of Magnetite (Fe3O4) and its Transition Point at Low Temperatures. *Nature* **1939**, *144*, 327-328.

[5] Verwey, E. J. W.; Heilmann, E. L. Physical properties and cation arrangement of oxides with spinel structures I. Cation arrangement in spinels. *J. Chem. Phys.* **1947**, *15*, 174-180.

[6] Fdez-Gubieda, M. L.; Muela, A.; Alonso, J.; García-Prieto, A.; Olivi, L.; Fernández-Pacheco, R.; Barandiarán, J. M. Magnetite Biomineralization in Magnetospirillum Gryphiswaldense: Time-Resolved Magnetic and Structural Studies. *ACS nano* **2013**, *7*, 3297-3305.

[7] Guo, X.; Chen, F. Removal of Arsenic by Bead Cellulose Loaded with Iron Oxyhydroxide from Groundwater. *Environ. Sci. Technol.* **2005**, *39*, 6808-6818.

[8] Yusan, S. D.; Akyil, S. Sorption of Uranium (VI) from Aqueous Solutions by Akaganeite. *J. Hazard. Mater.* **2008**, *160*, 388-395.

[9] Dutcher, B.; Fan, M.; Leonard, B.; Dyar, M. D.; Tang, J.; Speicher, E. A., Liu, P.; Zhang, Y. Use of Nanoporous FeOOH as a Catalytic Support for $NaHCO_3$ Decomposition Aimed at Reduction of Energy Requirement of Na_2CO_3/$NaHCO_3$ Based CO_2 Separation Technology. *J. Phys. Chem. C* **2011**, *115*, 15532-15544.

[10] Mackay, A. L. Beta-Ferric Oxyhydroxide. *Min. Mag.* **1960**, *32*, 545-557.

[11] Mackay, A. L. Beta-Ferric Oxyhydroxide-Akaganéite. *Min. Mag.* **1962**, *33*, 270-280.

[12] Murad, E. Mössbauer and X-ray Data on β-FeOOH (Akaganéite). *Clay Min.* **1979**, *14*, 273-283.

[13] Post, J. E.; Buchwald, V. F. Crystal Structure Refinement of Akaganeite. *Am. Miner.* **1991**, *76*, 272-277.

[14] Ståhl, K.; Nielsen, K.; Jiang, J.; Lebech, B.; Hanson, J. C.; Norby, P.; van Lanschot, J. On the Akaganéite Crystal Structure, Phase Transformations and Possible Role in Post-Excavational Corrosion of Iron Artifacts. *Corrosion Sci.* **2003**, *45*, 2563-2575.

[15] Post, J. E.; Heaney, P. J.; Von Dreele, R. B.; Hanson, J. C. Neutron and Temperature-Resolved Synchrotron X-ray Powder Diffraction Study of Akaganéite. *Am. Miner.* **2003**, *88*, 782-788.

[16] Barrero, C. A.; García, K. E.; Morales, A. L.; Kodjikian, S.; Greneche, J. M. New Analysis of the Mössbauer Spectra of Akaganeite. *J. Phys.: Condens. Matter* **2006**, *18*, 6827-6840.

[17] Chambaere, D. G.; De Grave, E.; Vanleerberghe, R. L.; Vandenberghe, R. E. The electric Field Gradient at the Iron Sites in β-FeOOH. *Hyperfine Interact.* **1984**, *20*, 249-262.

[18] Kulgawcz, D. S.; Obuszko, Z.; Szytula, A. Susceptibility and Magnetization of Beta- and Delta-FeOOH. *Phys. Stat. Sol.* **1968**, *26*, K-83.

[19] Urtizberea, A.; Luis, F.; Millán, A.; Natividad, E.; Palacio, F.; Kampert, E.; Zeitler U. Thermoinduced Magnetic Moment in Akaganéite Nanoparticles. *Phys. Rev. B* **2011**, *83*, 214426.

[20] Dézsi, I.; Keszthelyi, L.; Kulgawczuk, D.; Molnár, B.; Eissa, N.A. Mössbauer Study of ß- and δ-FeOOH and their Disintegration Products. *Phys. Stat. Sol.* **2011**, *22*, 617-628.

[21] Millan, A.; Urtizberea, A.; Natividad, E.; Luis, F.; Silva, N. J. O.; Palacio, F.; Ruiz-González, M.L.; González-Calbet, J. M.; Lecante, P.; Serin, V.; et al. Akaganéite Polymer Nanocomposites. *Polymer* **2009**, *50*, 1088–1094.

[22] Chambaere, D. G.; De Grave, E. The β-FeOOH to α-Fe2O3 Phase Transformation: Structural and Magnetic Phenomena. *Phys. Chem. Miner.* **1985**, *12*, 176-184.

[23] Coey, J. M. D. Interpretation of the Mössbauer Spectra of Speromagnetic Materials. *J. Phys.: Condens. Matter* **1993**, 5, 7297-7300.

[24] Brayner, R.; Yépremian, C.; Djediat, C.; Coradin, T.; Herbst, F.; Livage, J.; Fiévet, F.; Counté, A. Photosynthetic Microorganism-Mediated Synthesis of Akaganeite (β-FeOOH) nanorods. *Langmuir* **2009**, *25*, 10062-10067.

[25] Néel L. In Low temperature physics. Dewitt C.; Dreyfuss B.; de Gennes P. D. Editors. **1962**. New York: Gordon & Breach. p. 413.

[26] Richmond, W. R.; Cowley, J. M.; Parkinson, G. M.; Saunders, M. An Electron Microscopy Study of β-FeOOH (akaganéite) Nanorods and Nanotubes. *CrystEngComm* **2006**, *8*, 36–40.

[27] Cullity, B. D.; Stock, S. R. Elements of X-ray Diffraction. Prentice Hall. **2001**. 3rd Edition.

[28] Morrish, A. H. The Physical Principles of Magnetism. Wiley. **1965**. New York. pp. 680.

[29] Mørup, S.; Frandsen, C. Thermoinduced Magnetization in Nanoparticles of Antiferromagnetic Materials. *Phys. Rev. Lett.* **2004**, *92*, 217201.

[30] Cullity, B. D.; Graham, C. D. Introduction to Magnetic Materials. Wiley-IEEE Press. **2008**. 2nd Edition.

[31] Zysler, R. D.; Fiorani, D.; Testa, A. M. Investigation of Magnetic Properties of Interacting Fe_2O_3 nanoparticles. *J. Magn. Magn. Mat.* **2001**, *224*, 5-11.

[32] Carter, C. B.; Norton, M. G. Ceramic Materials: Science and Engineering Springer, **2007**.

pp 607.

[33] Del Bianco, L.; Fiorani, D.; Testa, A. M.; Bonetti, E.; Savini, L.; Signoretti, S. Magnetothermal Behavior of a Nanoscale Fe/Fe Oxide Granular System. *Phys. Rev. B* **2002**, *66*, 174418.

[34] Franco, V.; Pirota, K. R.; Prida, V. M.; Neto, A. M. J.; Conde, A.; Knobel, M.; Hernando, B.; Vázquez, M. Tailoring of Magnetocaloric Response in Nanostructured Materials: Role of Anisotropy. *Phys. Rev. B*. **2008**, *77*, 104434.

[35] Tiwari, S. D.; Rajeev, K. P. Signatures of Spin-Glass Freezing in NiO Nanoparticles. *Phys. Rev. B* **2005**, *72*, 104433.

[36] Luna, C.; Barriga-Castro, E. D.; Mendoza-Reséndez, R. The Effects of Aging Time on the Size, Morphology, Oriented Attachment and Magnetic Behavior of Hematite Nanocrystals Synthesized by Forced Hydrolysis of Fe^{III} Solutions. *Acta Mater.*. **2014**, *66*, 405-413.

[37] Zheng, R. K.; Gu, H.; Xu, B.; Zhang, X. X. The Origin of the Non-Monotonic Field Dependence of the Blocking Temperature in Magnetic Nanoparticles. *J. Phys.: Condens. Matter* **2006**, *18*, 5905-5910.

[38] De Almeida, J. R. L.; Thouless, D. J. Stability of the Sherrington-Kirkpatrick Solution of a Spin Glass Model. *J. Phys A: Math. Gen.* **1978**, *11*, 983-990.

[39] Folch, B.; Larionova, J.; Guari, Y.; Molvinger, K.; Luna, C.; Sangregorio, C.; Innocenti, C. Caneschi, A.; Guérin, C. Synthesis and Studies of Water-Soluble Prussian Blue-Type Nanoparticles into Chitosan Beads. *Phys. Chem. Chem. Phys.* **2010**, *12*, 12760-12770.

[40] Topkaya, R.; Akman, Ö.; Kazan, S.; Aktaş, B.; Durmus, Z.; Baykal, A. Surface Spin Disorder and Spin-Glass-Like Behaviour in Manganese-Substituted Cobalt Ferrite Nanoparticles. *J. Nanopart. Res.* **2012**,*14*, 1-16.

[41] Friedman, J. R.; Voskoboynik, U.; Sarachik, M. P. Anomalous Magnetic Relaxation in Ferritin. *Phys. Rev. B* **1997**, *56*, 10793.

[42] Tejada, J.; Zhang, X. X.; Del Barco, E.; Hernandez, J. M.; Chudnovsky, E. M. Macroscopic Resonant Tunneling of Magnetization in Ferritin. *Phys. Rev. Lett.* **1997**, *79*, 1754-1757.

[43] Usov, N. A. Numerical Simulation of Field-Cooled and Zero Field-Cooled Processes for Assembly of Superparamagnetic Nanoparticles with Uniaxial Anisotropy. *J. Appl. Phys.* **2011**, *109*, 023913.

[44] Serantes, D.; Baldomir, D.; Pereiro, M.; Arias, J. E.; Mateo-Mateo, C.: Buján-Núñez, M. C.; Vázquez-Vázquez, C.; Rivas, J. Interplay Between the Magnetic Field and the Dipolar Interaction on a Magnetic Nanoparticle System: A Monte Carlo Study. *J. Non-Cryst. Solids* **2008***, 354*, 5224-5226.

[45] O'Grady, K.; Chantrell, R.W.; Studies of Magnetic Properties and their Relevance to Materials Science. Edited by J.L. Dormann, D. Fiorani. Elsevier Sci. Publ., 1992, p. 93.

[46] Zysler, R. D.; Vasquez Mansilla, M.; Fiorani, D. Surface Effects in α-Fe$_2$O$_3$ Nanoparticles. *Eur. Phys. J. B* **2004**, *41*, 171-175.

[47] Folch, B.; Guari, Y.; Larionova, J.; Luna, C.; Sangregorio, C.; Innocenti, C.; Caneschi, A.; Guérin, C. Synthesis and Behaviour of Size Controlled Cyano-Bridged Coordination Polymer Nanoparticles within Hybrid Mesoporous Silica. *New J. Chem.* **2008**, *32*, 273-282.

[48] Seo, W. S.; Jo, H. H.; Lee, K.; Kim, B.; Oh, S. J.; Park, J. T. Size‑Dependent Magnetic Properties of Colloidal Mn$_3$O$_4$ and MnO Nanoparticles. *Angew. Chem. Int. Ed.* **2004**, *43*, 1115-1117.

[49] del Barco, E.; Duran, M.; Hernandez, J.M.; Tejada, J.; Zysler, R. D.; Vasquez Mansilla, M.; Fiorani, D. Magnetic Relaxation Measurements of α-Fe$_2$O$_3$ Antiferromagnetic Particles Below 1 mK. *Phys. Rev. B* **2002**, *65*, 052404.

[50] Bontemps, N.; Rajchenbach, J.; Chamberlin, R. V.; Orbach, R. Dynamic Scaling in the Eu 0.4Sr0.6S Spin-Glass. *Phys. Rev. B* **1984**, *30*, 6514-6520.

[51] Larionova, J.; Guari, Y.; Tokarev, A.; Chelebaeva, E.; Luna, C.; Sangregorio, C.; Caneschi; A.; Guérin, C. Coordination Polymer Nano-Objects into Ionic Liquids: Nanoparticles and Superstructures. *Inorg. Chim. Acta* **2008**, *361*, 3988-3996.

[52] Nogués, J.; Schuller, I. K. Exchange bias. *J. Mag. Mag. Mat.* **1999**, *192*, 203-232.

[53] Ong, Q. K.; Wei, A.; Lin, X.-M. Exchange Bias in FeO/Fe$_3$O$_4$ Core-Shell Magnetic Nanoparticles Mediated by Frozen Interfacial Spins. *Phys. Rev. B* **2009**, *80*, 134418.

[54] Ammar, S.; Helfen, A.; Jouini, N., Fievet, F.; Rosenman, I.; Villain, F.; Molinie, P.; Danot, M. Magnetic Properties of Ultrafine Cobalt Ferrite Particles Synthesized by Hydrolysis in a Polyol Medium. *J. Mater. Chem.* **2001**, *11*, 186-192.

[55] Calero-DdelC, V. L.; Rinaldi, C. Synthesis and Magnetic Characterization of Cobalt-Substituted Ferrite (Co$_x$Fe$_{3-x}$O$_4$) Nanoparticles. *J. Mag. Mag. Mat.* **2007**, *314*, 60–67.

[56] Dimitrov, D. A.; Wysin, G. M. Effects of Surface Anisotropy on Hysteresis in Fine Magnetic Particles. Phys. Rev. B **1994**, *50*, 3077-3084.

FIGURES
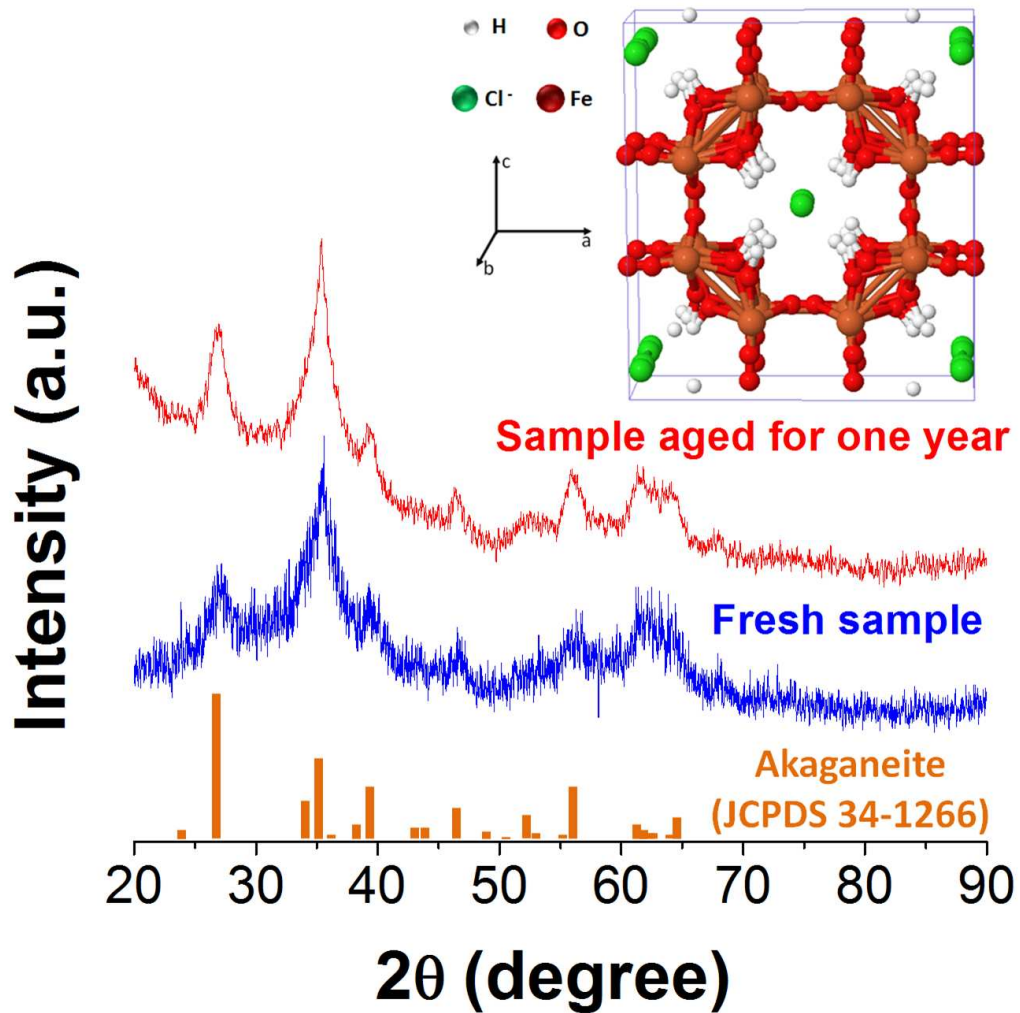
Figure 1 XRD pattern of ultra-fine akaganéite nanoparticles (before and after the aging process at room temperature during one year). The inset shows a schematic ball-and-stick representation of the akaganéite unit cell (monoclinic I2/m representation). This arrangement displays square channels that are occupied by chloride ions that stabilize the structure.
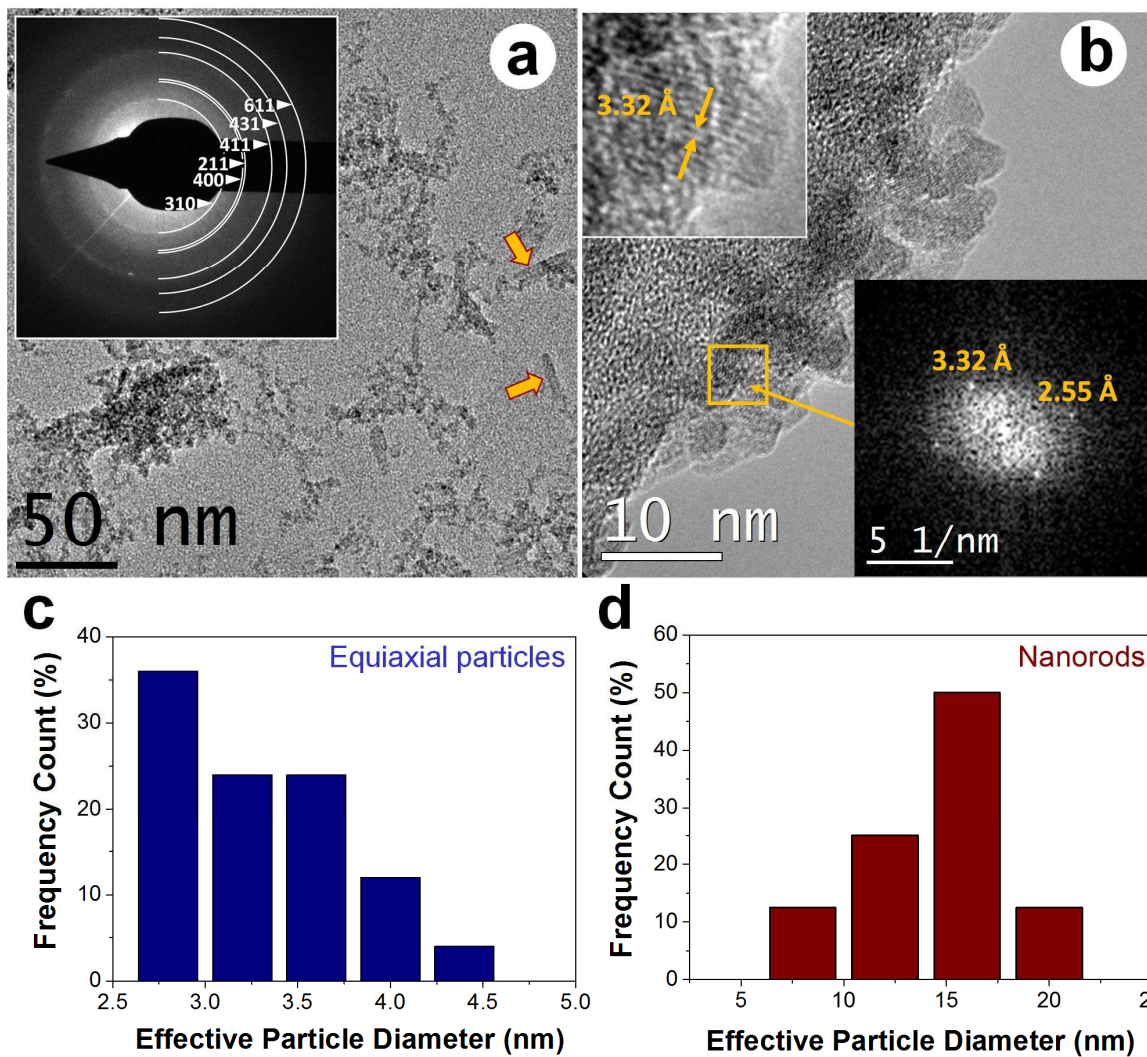
Figure 2 a) TEM micrograph of the akaganéite nanoparticles at low magnification. The inset shows the SAED pattern of the large-area showed in panel a) of the Figure. The presence of rod-like shape nanoparticles is highlighted by arrows. b) HRTEM image. Above inset is a magnification of the image. Below inset is the FFT pattern of the area highlighted by square. c) and d) Histograms of the effective particle diameter of the equiaxial particles and nanorods observed in the TEM micrographs.
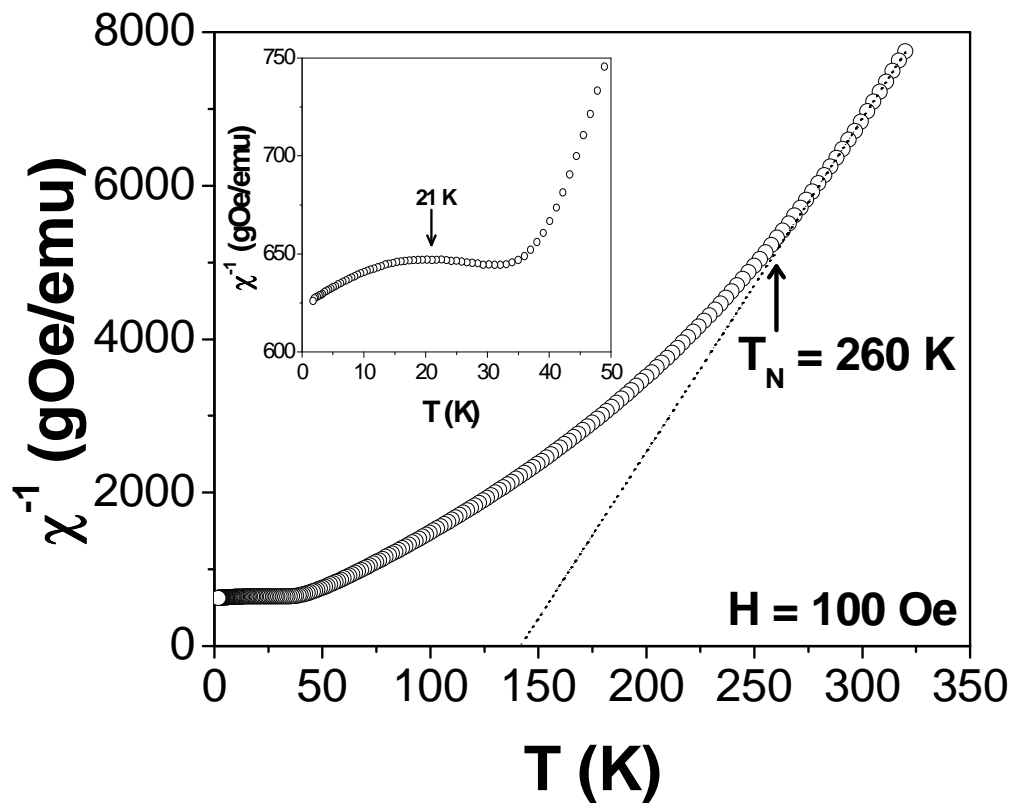
Figure 3 Thermal dependence of the inverse of the dc magnetic susceptibility of the sample measured in a constant magnetic field of 100 Oe. The dot line represents the best fit curve to equation (4) in the temperature range from 295 to 320 K. The fitting parameters are C=0.024(2) emu K Oe^{-1} g^{-1} and θ = 133(1) K. The inset represents the 1/χ vs T curve at low temperatures.
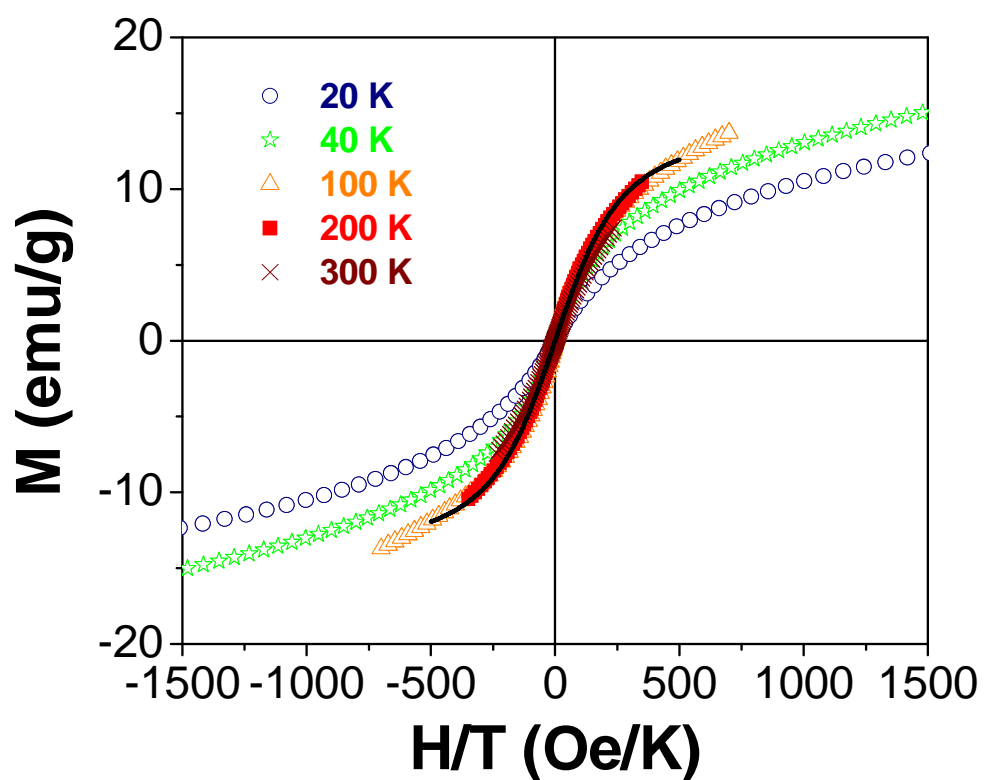
Figure 4 Experimental magnetization versus H/T curves obtained at different temperatures. The best fit curve to equation (5) is represented by black solid line.
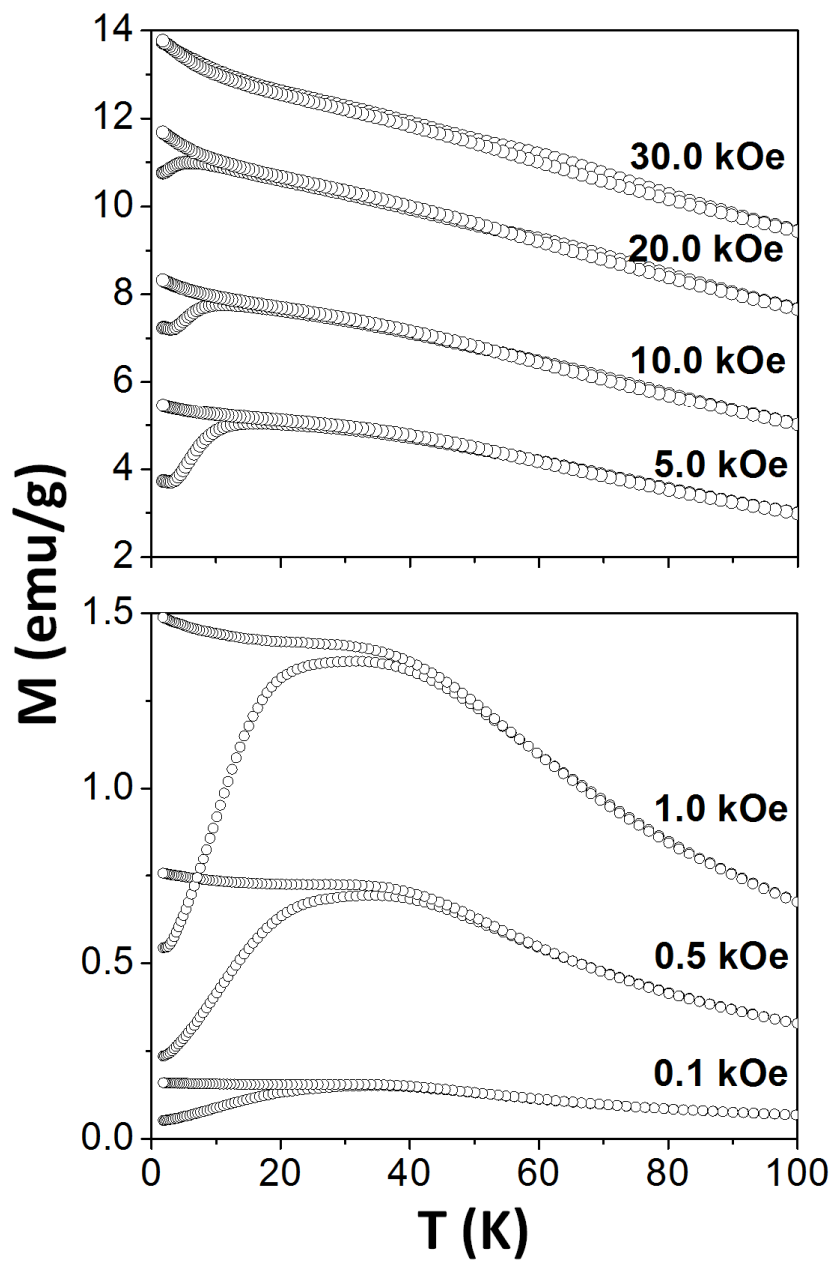
Figure 5 Zero-field cooled and field cooled magnetization curves obtained at different applied fields.
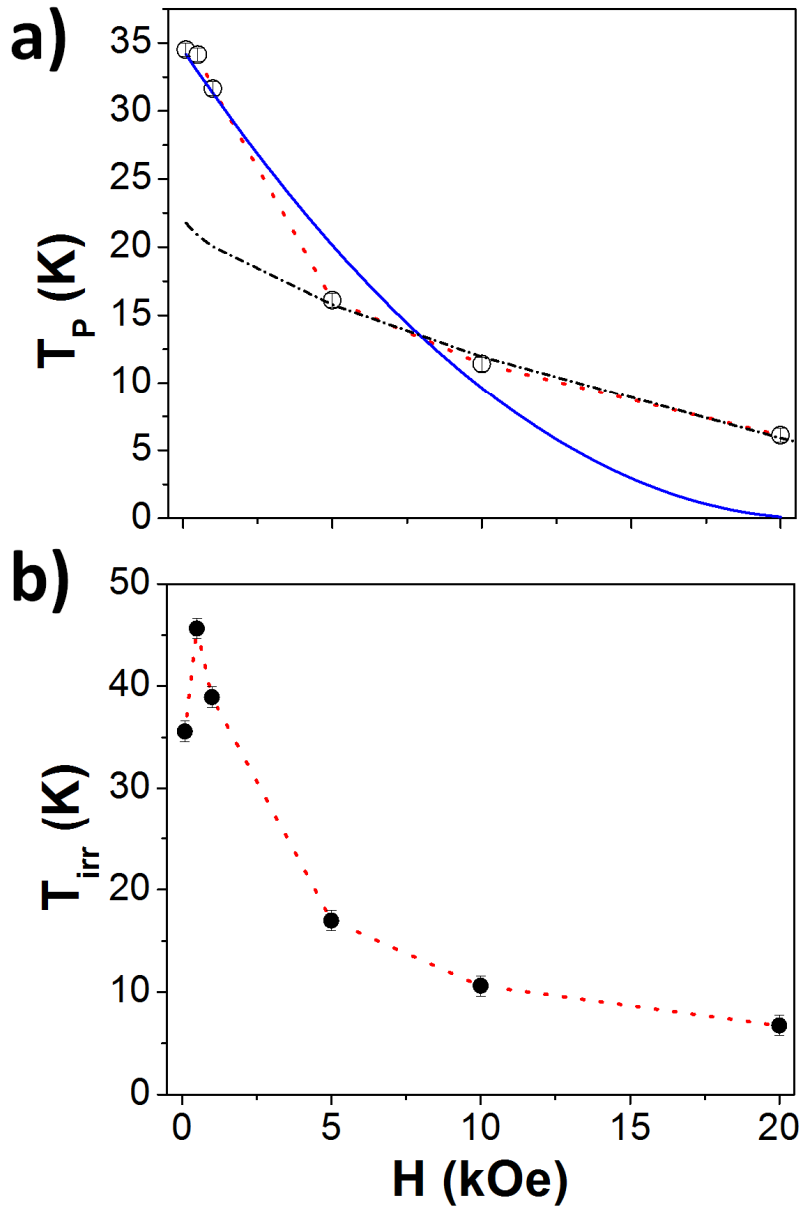
Figure 6 Dependence of (a) the temperature at which the ZFC magnetization curve reach a peak and (b) the irreversibility temperature of the ZFC-FC curves on the exciting dc magnetic field. The solid blue curve is the best fit curve to equation (6) assuming equation (7). The dashed black curve corresponds to the best fit to equation (8). Red dotted curves are just guides to the eye.
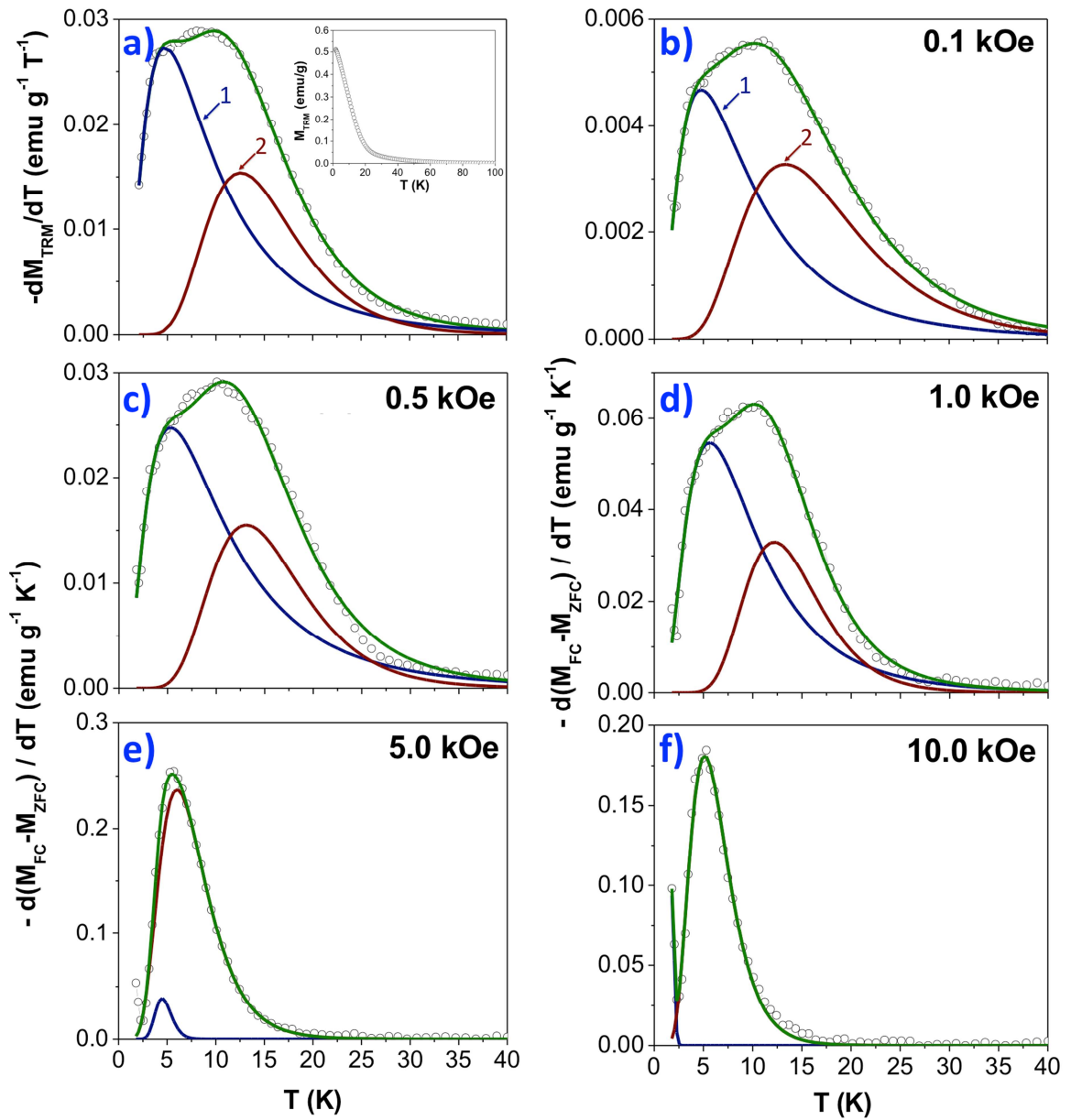
Figure 7 a) Thermoremanent magnetization (M_{TRM}) curve measured at 100 Oe (inset) and its temperature derivative, $-dM_{TRM}/dT$. b)-f) Thermal dependence of the derivative of the difference M_{FC} - M_{ZFC} with respect to temperature obtained at different magnetic fields. The green curve is the best curve fit to the sum of two log-normal distributions (curves in blue and red, named 1 and 2 respectively).
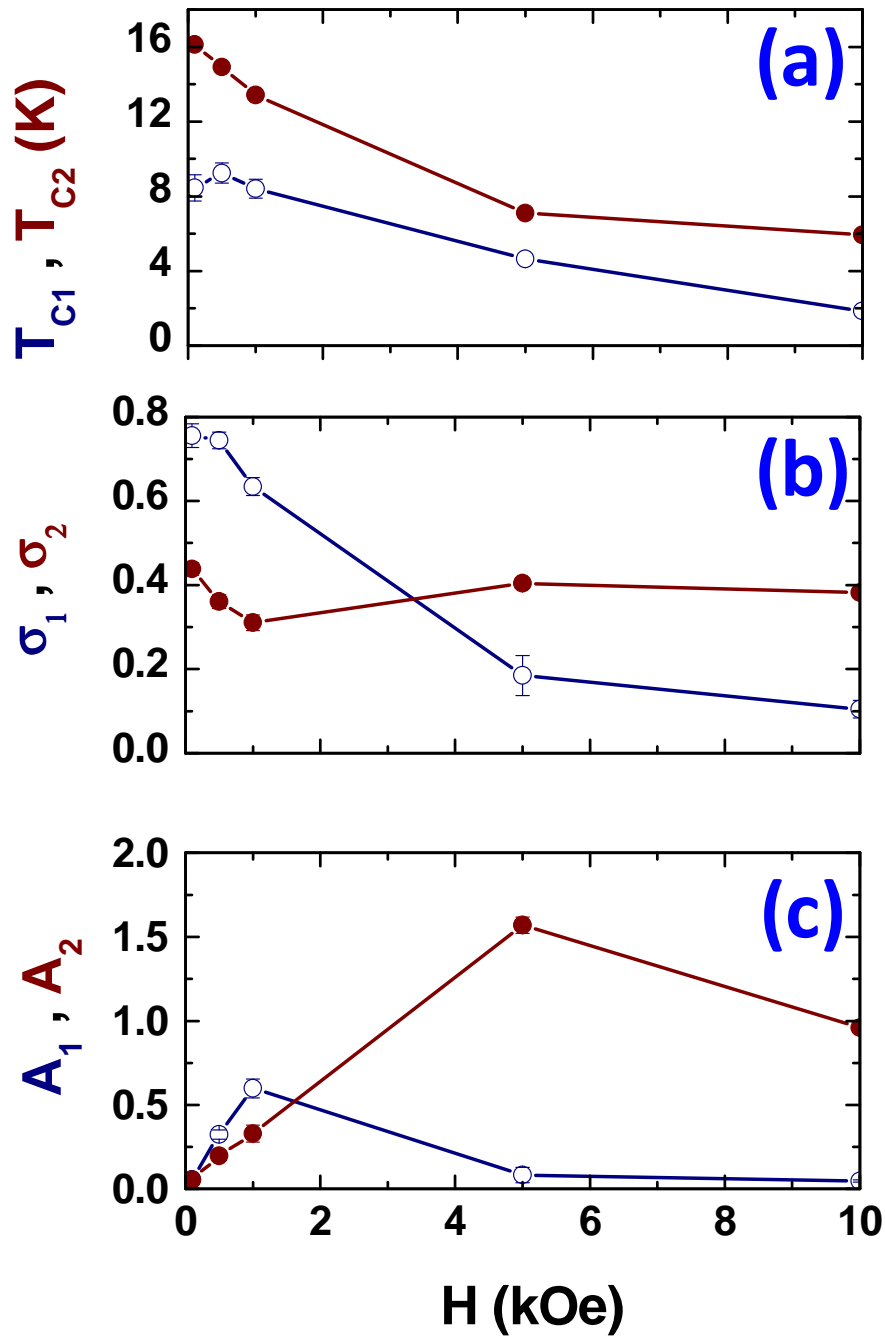
Figure 8 Field dependences of the parameters obtained with the fits presented in Figure 7: a) central values, b) standard deviations and c) amplitude values of the log-normal distributions 1 and 2.
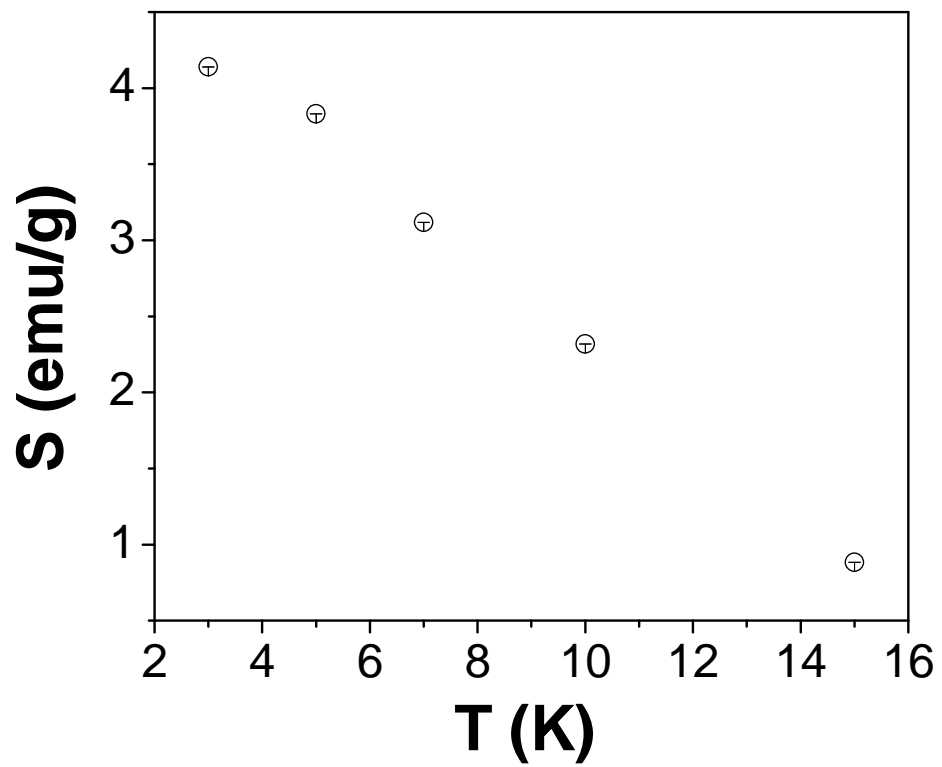
Figure 9 Thermal dependence of the magnetic viscosity.
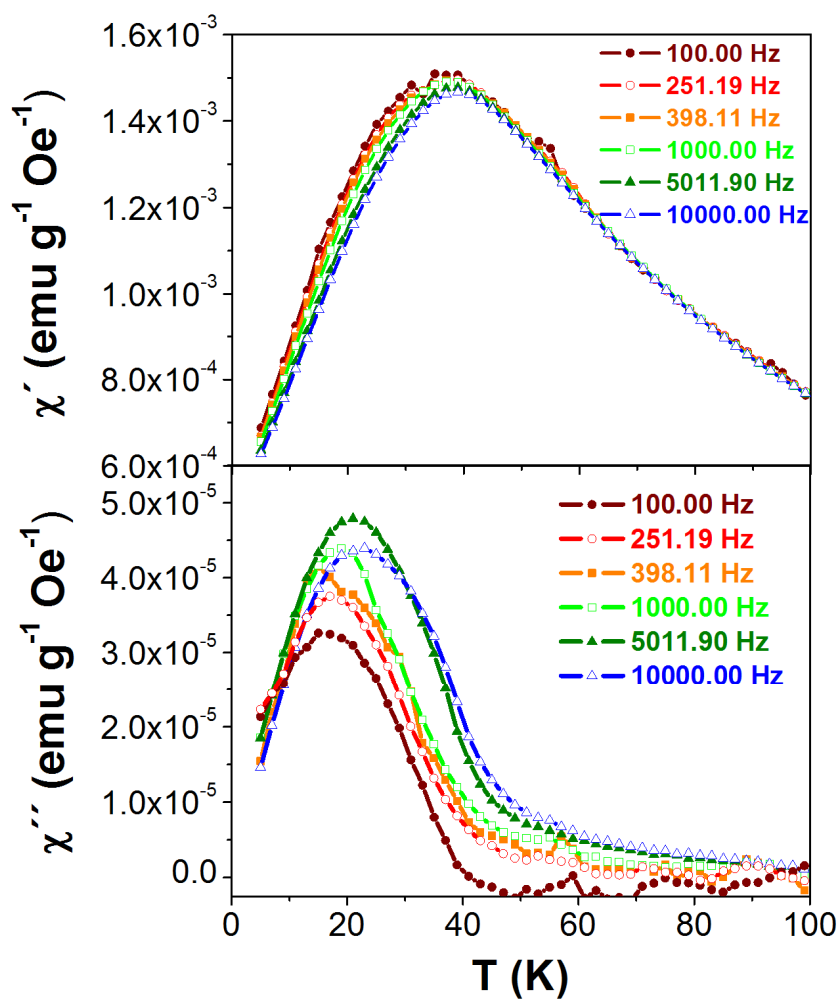
Figure 10 Thermal dependence of the (a) real and (b) imaginary parts of the AC susceptibility of the akaganéite nanoparticles obtained at different frequencies of the exciting magnetic field.
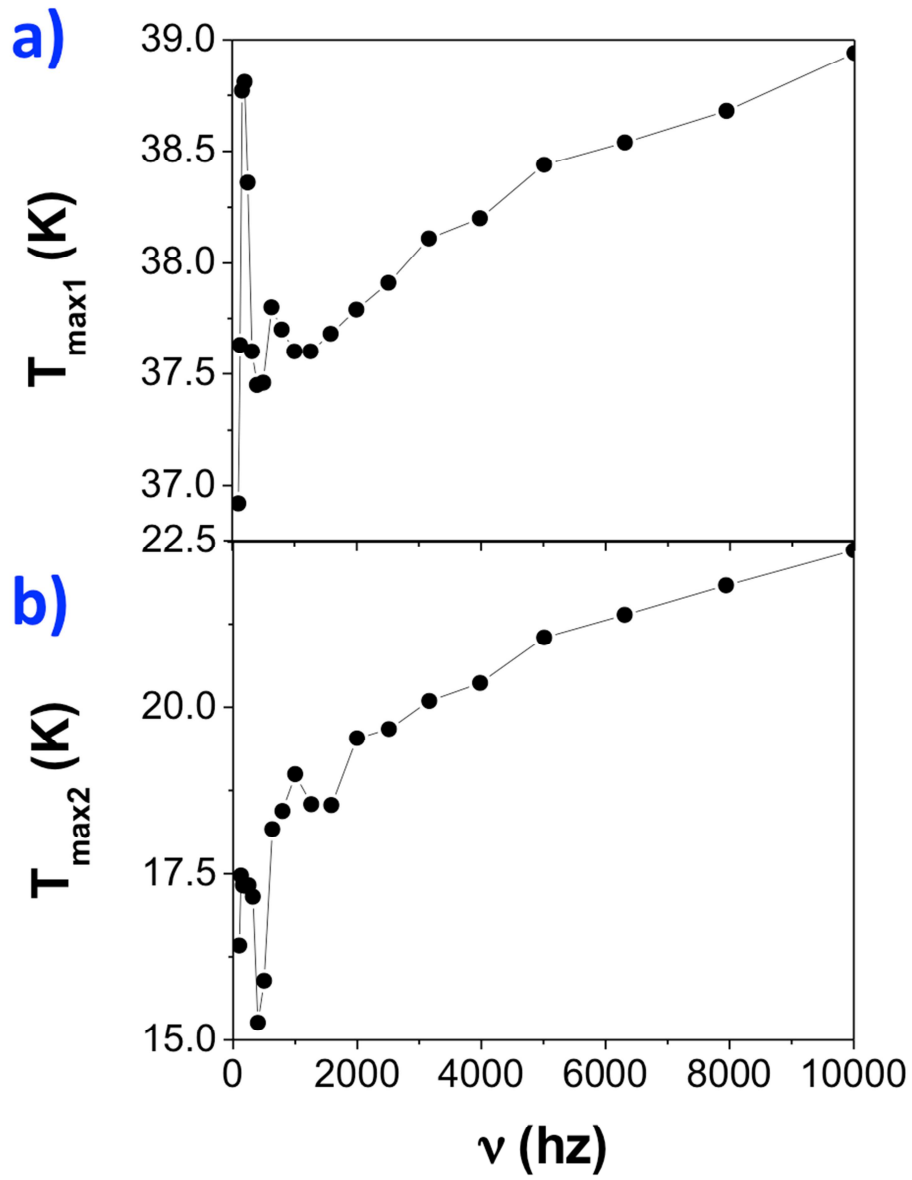
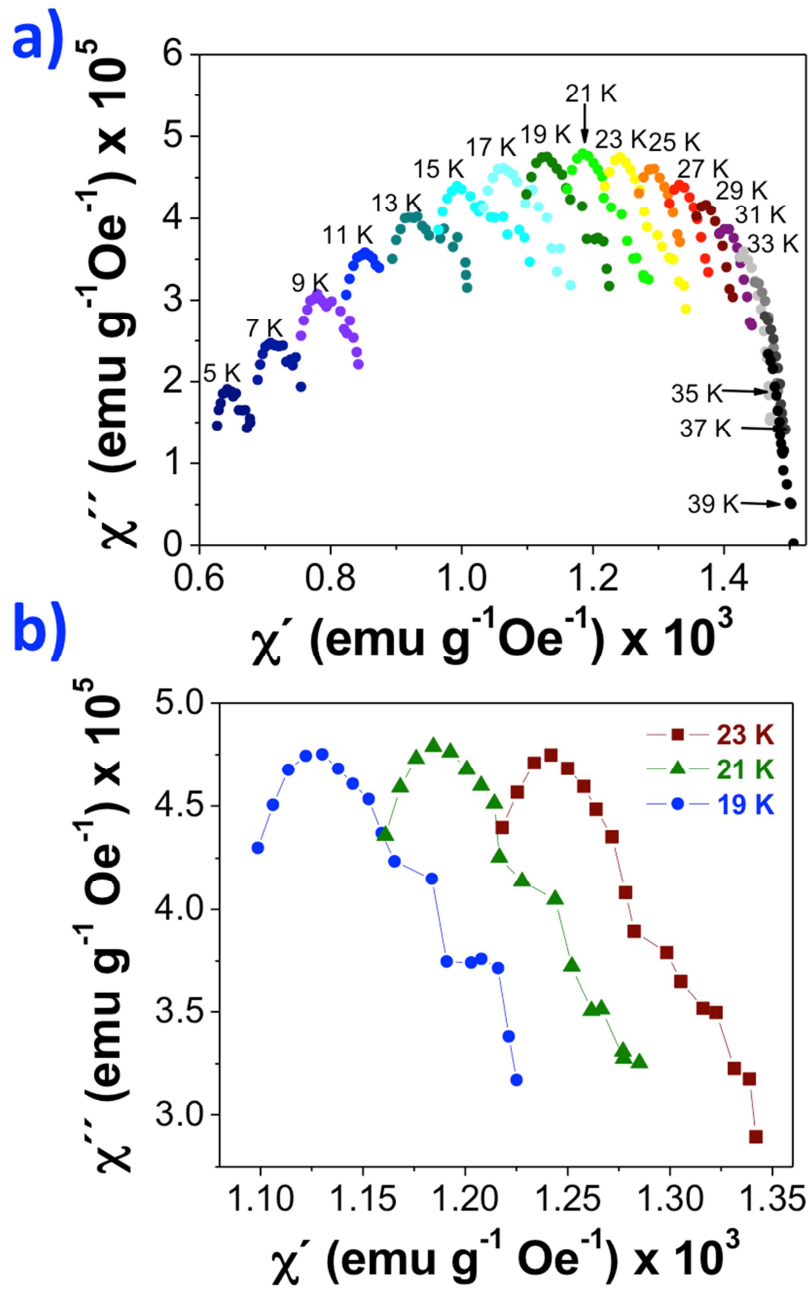**Figure 11** Frequency dependence of the cusp temperatures of a) χ' and b) χ''.

Figure 12- a) Cole-Cole plots obtained at temperatures from 5 up to 39 K. b) Cole-Cole plots obtained at selected temperatures (19, 21, 23 K).
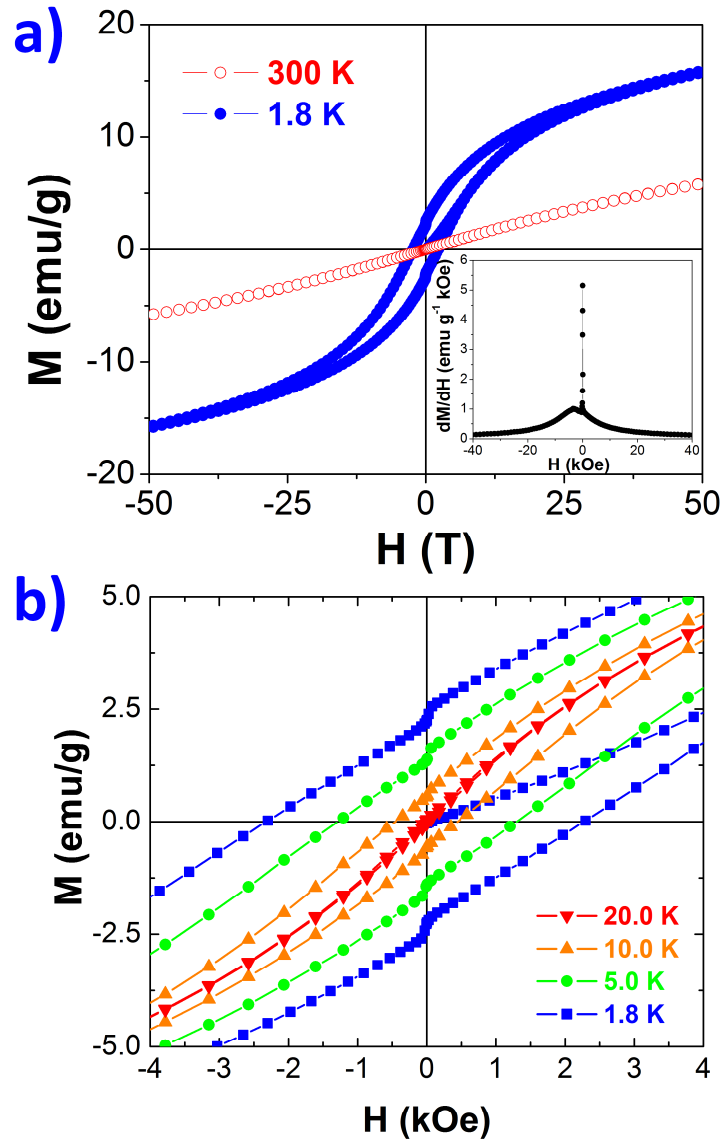
Figure 13 a) Field-dependence of the magnetization obtained at different temperatures. The inset shows the field dependence of the field derivative of one of the branch of the hysteresis loops measured at 1.8 K. b) Low field region of the hysteresis loops measured at 1.8, 5, 10 and 20 K.
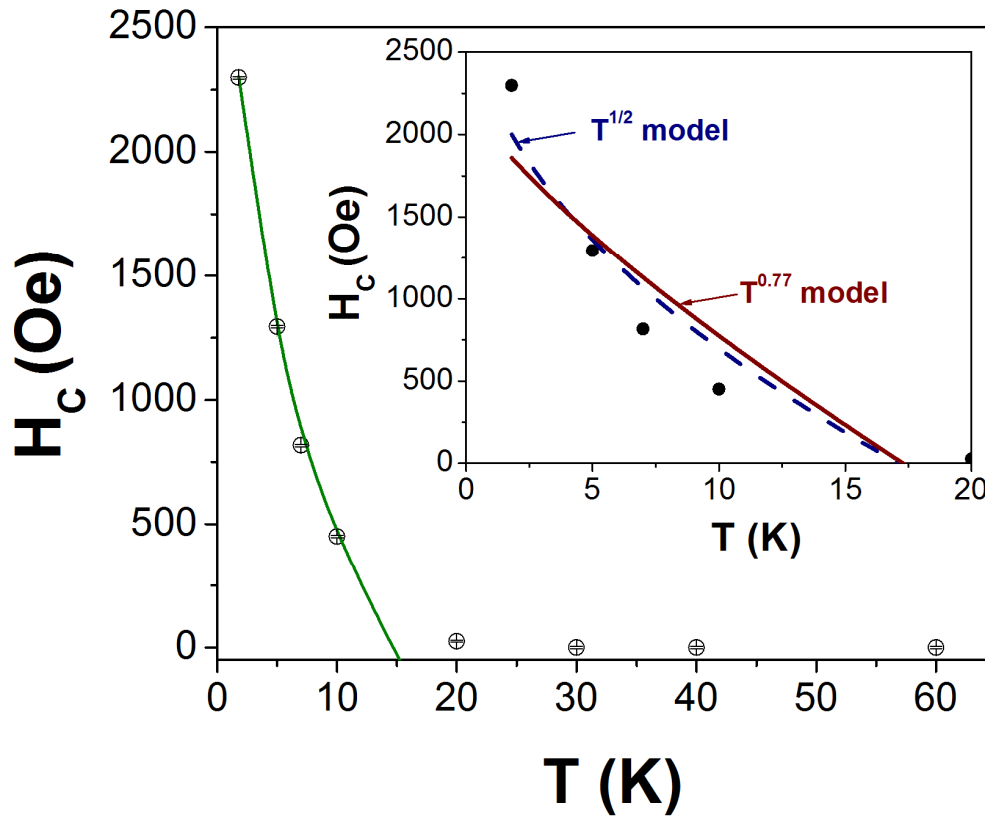
Figure 14 Temperature dependence of the coercive field. The green curve corresponds to the fit of the experimental data to equation (11) with k as a free fit parameter. Inset shows the experimental data (black points) and the best fit curves for $T^{1/2}$ (dashed line) and $T^{0.77}$ (continuous line) models, respectively. The parameters obtained from these fits were $H_C(0) = 2,962(395)$ Oe, $T_B = 17(2)$ K for the $T^{1/2}$ model and $H_C(0) = 2,255(370)$ Oe, $T_B = 17(3)$ K for the $T^{0.77}$ model. The coefficients of determination R^2 were 0.90592 and 0.83918, respectively.